CONF-910617--4

DE92 000043

MECHANICAL PROPERTIES AND MICROSTRUCTURE OF PRESSURELESS SINTERED DUOPHASE SIALON

Ran-Rong Lee, Bruce E. Novich, George Franks, Debbie Ouellette
Ceramics Process Systems Corporation
Milford, MA 01757, USA
Mattison K. Ferber, Camden R. Hubbard, and Karren More
High Temperature Materials Laboratory
Oak Ridge National Laboratory
Oak Ridge, TN 37831, USA

ABSTRACT

Duophase (α'/β') sialon is being developed for ceramic engine applications by using the Quickset™ injection molding process, followed by pressureless sintering and a thermal treatment. The sialon had an average four-point flexural strength of 670 MPa at room temperature and 490 MPa at 1370°C. It survived the flexural stress rupture test at 1300°C and 340 MPa for 190 hours. X-ray diffraction (XRD) and transmission electron microscopy (TEM) characterization showed that crystallization of the grain boundary phase improved the high temperature flexural strength of this sialon material. The creep behavior was also found to be affected by the crystallized grain boundary phases. The formation of a yttrium aluminum garnet (YAG) phase and elongated grains yielded better creep resistance. The correlation between mechanical properties and microstructure is discussed.

INTRODUCTION

Silicon nitride (Si_3N_4) is one of the prime candidate materials for high temperature ceramic turbine engine applications.[1] Most of the high performance silicon nitrides used in the Advanced Turbine Technology Applications Project (ATTAP) require hot-isostatic-pressing (HIP) to achieve high density and good mechanical properties. Two important issues related to the HIPped silicon nitride need to be addressed: 1) HIP is a very expensive process, and is thus not a cost-effective manufacturing process for ceramic engine components and 2) the mechanical properties of silicon nitride with an as-HIPped surface are worse than that with an as-machined surface,[2] probably due to the glass reaction layer on the as-HIPped surface resulting from the glass encapsulation process. In comparison, pressureless sintering is a lower cost manufacturing process and does not require glass-encapsulation. However, to achieve full density, greater amounts of sintering aids must be employed for

pressureless sintered ceramics. Typically, the high temperature mechanical properties and oxidation resistance of pressureless-sintered silicon nitride are greatly reduced by the increased amounts of grain boundary phases generated form the sintering aids.

Several techniques involving the modification of the grain boundary phases have been used to improve the high temperature mechanical properties. They can be classified into the following approaches: (1) Decrease the amount of the grain boundary phase by using less or no sintering aid. However, this method requires glass-encapsulation HIP or hot-pressing to achieve high density.[3] (2) Increase the viscosity of the glassy grain boundary phase by using more refractory sintering aids such as yttria, instead of magnesia (3) Crystallize the grain boundary phase.[4] (4) Diffuse some of the elements within the grain boundary phase into the matrix grains during densification.[5] For the pressureless-sintered material examined in this study, the focus was on approaches (2), (3) and (4).

Beta silicon aluminum oxynitride (β'-sialon), formed from the liquid phase sintering of silicon nitride with the addition of yttria and alumina, has been under development for more than a decade for cutting tool, extrusion die and other engineering applications. However, the application of β' sialon in the ceramic turbine engine was limited by the degradation of the grain boundary phase at temperatures exceeding 1200°C, similar to other types of pressureless-sintered silicon nitride materials. Recently, the duophase (α'/β') sialon material was found to perform very well in cutting tool applications.[6] The purpose of this study is to develop the duophase (α'/β') sialon for ceramic engine applications. This paper reports the room temperature and high temperature mechanical properties of the duophase sialon and their correlation with microstructure and processing. The focus is on grain boundary engineering for improving the high temperature mechanical properties through the post-sintering treatment.

MATERIALS AND METHODS

Materials Preparation

The duophase sialon was prepared from silicon nitride powder with optimum amounts of yttria (Y_2O_3) and 21R ($SiAl_6O_2N_6$) as sintering aids. The green billets having dimensions of 25 mm x 50 mm x 9.4 mm were produced using the Quickset™ injection process, which is the forming process for engine component fabrication at Ceramics Process Systems Corporation. The details of the forming process are described elsewhere.[7,8] The green parts were sintered in a graphite furnace in a flowing nitrogen atmosphere. The nitrogen pressure was only slightly higher than ambient pressure. The post-sintering thermal treatment was carried out in the same furnace, but at lower temperatures. Three different batches of samples, #G, #H and #I, having the same composition, but different firing cycles, are evaluated in this paper.

Mechanical Testing

The flexural strength was measured by using a four-point loading fixture following MIL-STD-1942(MR) specification. The "A" bar configuration, with a specimen size of 1.5 x 2 x 30 mm, was used for measuring the room temperature flexural strength and the "B" bar configuration, with a size of 3 x 4 x 50 mm, was used for the high temperature flexural strength and stress rupture testing. The loading rate for the room temperature flexural

testing was 0.2 mm/min and that for the high temperature flexural testing was 5 lb/s. The room temperature fracture toughness was measured by using the controlled-flaw strength method.[9]

The flexural creep tests were conducted using a SiC four-point fixture having inner and outer spans of 20 and 40 mm, respectively. During the testing, an LVDT tracked the downward displacement of the load ram. A computer monitored this displacement as well as the load on each specimen and provided necessary adjustments to maintain the desired stress level.

The calculation of the tensile creep strain from the flexural strain data was based on the formulation of Hollenburg.[10] The creep behavior generated from the flexure test are described by the equation,[11]

$$d\varepsilon_s/dt = A_o(\sigma_a/\sigma_o)^n$$

where $d\varepsilon_s/dt$ is the steady-state creep rate, A_o is a pre-exponential factor, σ_a is the applied stress, σ_o is a normalizing parameter (=1 MPa), and n is the creep exponent.

TEM/EDS Characterization

Transmission electron microscopy (TEM) was used to identify the secondary phases and characterize the morphology of the grain boundary phases in each sample. TEM specimens were cut from the samples before and after creep deformation. The specimens were mechanically thinned to ~75 μm in thickness, dimpled down to ~25 μm in thickness and ion milled at 6 kV and 1 amp at 15°. The analytical electron microscopy (AEM) was performed at 200 kV in a JEOL 2000FX equipped with a Kevex Quantum ultra-thin window energy dispersive spectrometer (EDS).

X-ray diffraction (XRD)

X-ray diffraction was used to identify the intergrangular phases and α'/β' contents in the duophase sialons. The XRD system consisted of a Cu X-ray tube operated at 45 kV and 40 mA, 230 mm radius goniometer, and a Ge solid-state detector. Patterns were collected at 0.1°/min scanning rate. Phase identification was based on reference patterns contained in Sets 1-40 of the Powder Diffraction Files.

RESULTS

Mechanical/Thermal Properties

Flexural strength The four-point flexural strengths of the duophase sialon are plotted in Figure 1. The strength of the as-sintered material decreased gradually from 745 MPa at 25°C to 550 MPa at 1200°C, and then dropped to 350 MPa at 1300°C and 1370°C. In comparison, the duophase sialon after post-sintering thermal treatment had a lower room temperature flexural strength of 670 MPa, but maintained relatively good strength at high temperatures, having a flexural strength of 490 MPa at 1300°C and 1370°C. These results demonstrate the importance of the post-sintering thermal treatment on the mechanical properties of the duophase sialon.

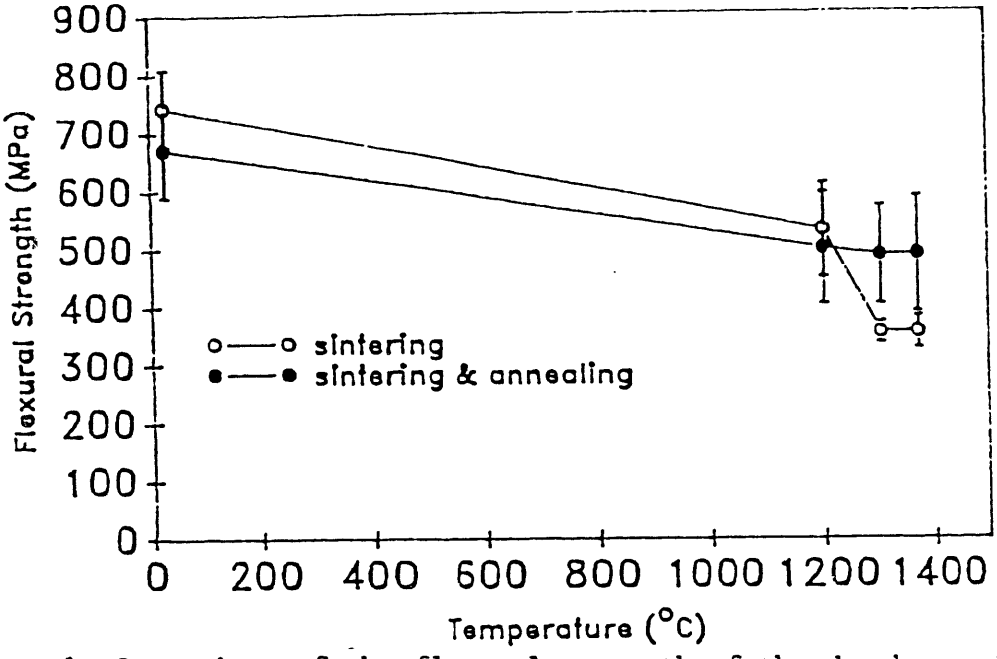

Figure 1. Comparison of the flexural strength of the duophase sialons before and after a post-sintering thermal treatment.

Flexural stress rupture The flexural stress rupture was tested at stresses of 240 MPa and 340 MPa at 1300°C. The strain verse time curves of the samples, #G, #H and #I, are plotted in Figure 2. At 240 MPa, samples #H and #I had better creep resistance than sample #G. When the stress was increased from 240 MPa to 340 MPa, #I showed better creep resistance than #H, indicating that sample #H was more sensitive to the applied stress. The secondary creep rates of the these samples tested at different conditions are summarized in Figure 3. Notice that the creep rate of sample #I was not as sensitive to the applied stress. From these data, the creep exponents (n) of #H and #I were calculated to be 2.7 and 0.7, respectively.

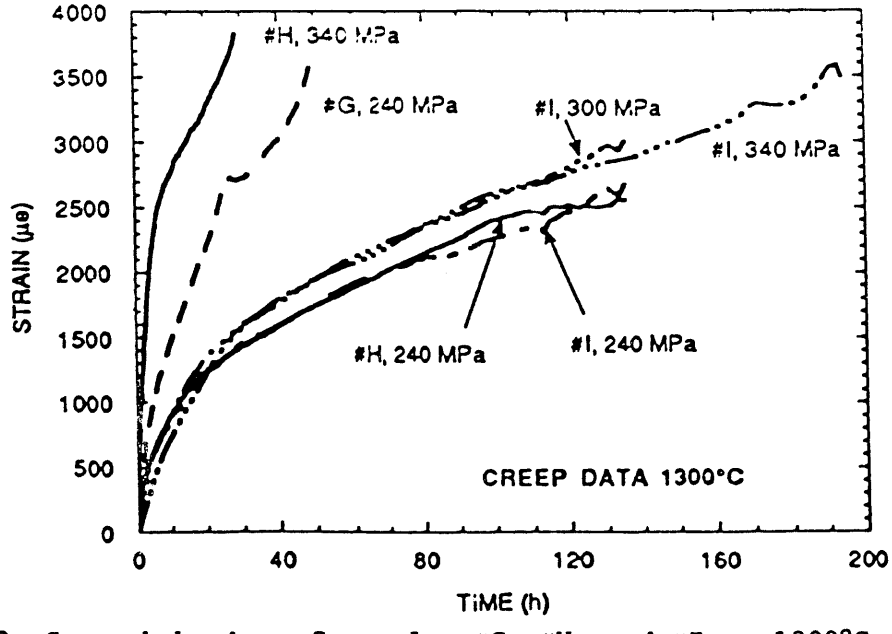

Figure 2. Creep behavior of samples #G, #H, and #I at 1300°C and several stress conditions

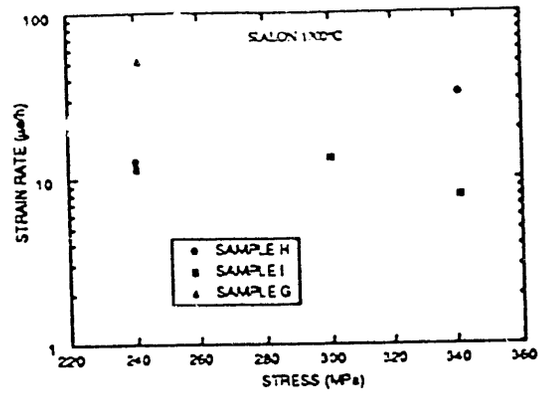

Figure 3. Secondary steady-state creep rates of samples #G, #H and #I under various conditions

Hardness The hardness, measured using a Vickers indenter, was 20.5 GPa, which was higher than the hardness of pure β' sialon of 17 GPa.[12]

Microstructure/Phase Characterization

The microstructure and phases of the sialon materials were characterized using XRD and AEM. In the as-sintered samples, the sialon had an amorphous grain boundary phase, as determined by electron diffraction. After a post-sintering heat treatment, the grain boundary phases were crystallized. In addition to equiaxed grains of both α' and β', elongated β' grains were observed, as shown in Figure 4. Several crystalline grain boundary pockets are arrowed in this figure.

Figure 4. TEM image showing typical microstructure of α'/β' sialon material (sample #I). Several crystalline grain boundary pockets are arrowed.

There were several microstructural/phase differences observed between the three batches of samples, #G, #H and #I, corresponding to the differences in creep behavior of these three samples. From XRD, the major difference between the #G, #H and #I was the α' and β' contents. #G had much less α' sialon (~19 %) than #H and #I (~37 %), and #G also was found to have fewer elongated β' grains than #H and #I. Among these three samples, #H had the highest amount of elongated grains. Two different

types of elongated grains were found in #H, the normal elongated β' grains and highly faulted elongated grains, as shown in Figure 5 (see morphology of the labelled grains and the inset electron diffraction pattern). From EDS, the faulted elongated grains were found to be a (high-Al)-Si-O-N (Figure 6(a)), as compared with the (high-Si)-Al-O-N β' sialon grains (Figure 6(b)). This (high-Al)-Si-Al-O-N phase was identified as ζ-$Si_3Al_7O_3N_9$[13] by XRD.

Figure 5. TEM image of sample #H showing elongated β' grains as well as elongated and highly faulted ζ-$Si_3Al_7O_3N_9$ grains (labelled). Diffraction pattern of a ζ-$Si_3Al_7O_3N_9$ grain is inset.

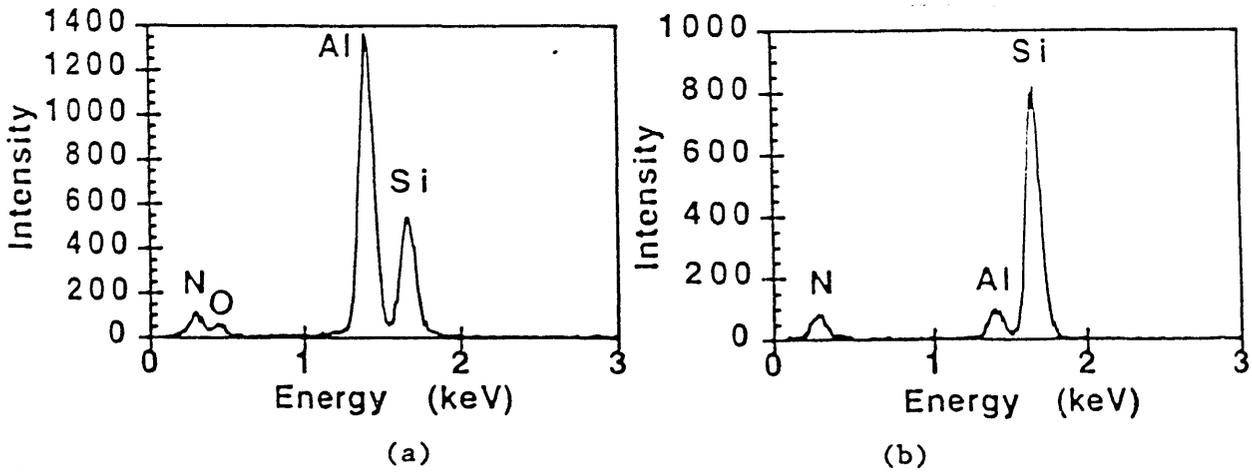

(a) (b)

Figure 6 EDS spectra from (a) an elongated ζ-$Si_3Al_7O_3N_9$ grain and (b) an elongated β' grain

The major grain boundary phase found in these three samples was a yttrium aluminum garnet (YAG) phase as identified by XRD. From EDS characterization, a small amount of silicon (Si) was found in the YAG phase ($Y_3Al_5O_{12}$). Thus, a Si-diffused YAG phase was formed. These YAG pockets were large enough such that any contribution to the Si from surrounding Si_3N_4 grains was minimized. Other minor grain boundary phases identified by XRD were K-phase ($YSiO_2N$) and melilite ($Y_2Si_3O_3N_4$). Sample #G appeared to have more of the Y-Si-O-N (K-phase or melilite) from AEM characterization.

Following creep testing, TEM samples were prepared from both the tensile and compressive faces of the test bars. Sample #G had many cracks at the tensile side of the specimen, with the cracks running perpendicular to the tensile face, as shown in Figure 7. In fact, TEM samples were extremely difficult to prepare from this sample as the surface repeatedly crumbled during the grinding and polishing steps. Samples #H and #I showed no obvious microstructural differences following creep. There were no microcracks and no cavitation was observed in either sample. The phases remained unchanged in each sample after creep at 1300°C, as determined by XRD.

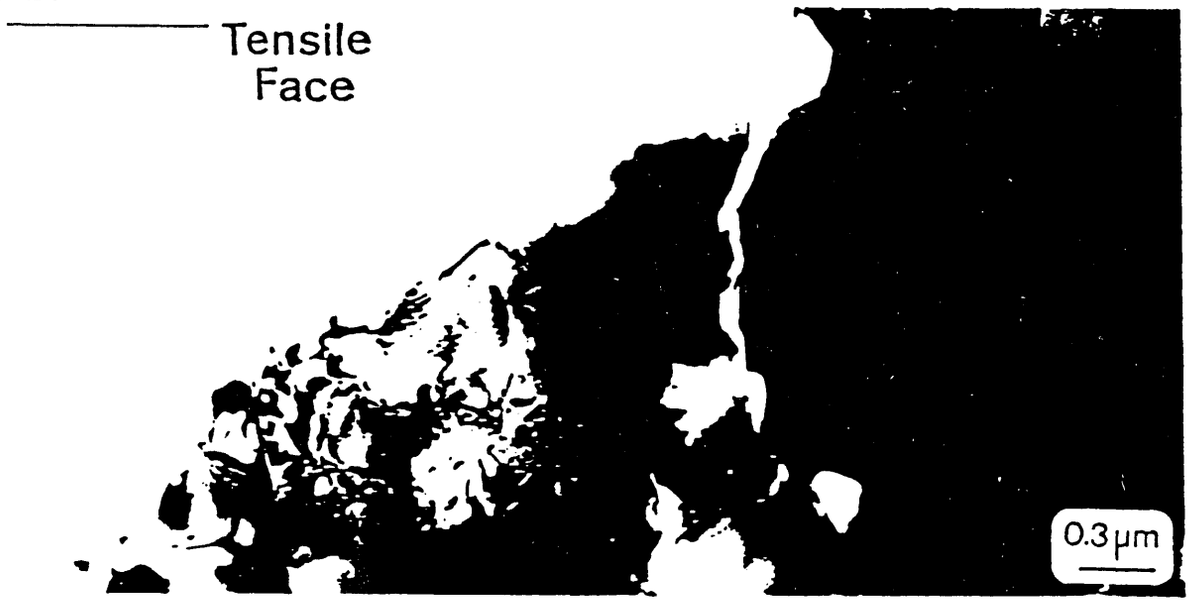

Figure 7. TEM image of #G after creep testing at 240 MPa and 1300°C, showing cracks running perpendicular to the tensile surface.

DISCUSSION

The improvement of the high temperature flexural strength of the duophase sialon after the post-sintering thermal treatment can be related to the crystallization of the grain boundary phases. The crystallized grain boundary phases also decreased the room temperature flexural strength, perhaps due to residual stresses resulting from the thermal expansion mismatch between the crystallized grain boundary phases and the sialon grains.

The creep behavior of the duophase sialon was also affected by the microstructure and grain boundary phases. Samples #G, #H, and #I, having the same formulation but different firing cycles, had quite different creep behaviors. Sample #G had the worst creep resistance and the lowest α' content. The smaller amount of α' phase in #G indicates that more yttrium was left in the grain boundary phases. Thus, more yttrium-containing grain boundary phases formed. The melilite and K-phases found in #G appeared to be more than that in #H and #I. Therefore, the creep resistance was worse than that of sample #H and #I. The elongated grains in sample #H and #I are also believed to improve the creep resistance. The creep resistances of #H and #I were close to each other at the lower stress (240 MPa), but #I material had better creep resistance at the higher stress (340 MPa). Further evaluation on the differences between these two samples is in progress.

The creep exponent (n) could be calculated using the equation

$\varepsilon_1/\varepsilon_2 = (\sigma_1/\sigma_2)^n$, where ε_1 and ε_2 are the strain rates and the σ_1 and σ_2 are the applied stresses. From the data in Figure 3, the stress exponents of samples #H and #I were calculated to be 2.7 and 0.7, respectively. Sample #H had a stress exponent larger than one, indicating that some creep mechanism, in addition to Coble diffusional creep, played an important role in the creep behavior of this material. Sample #I had a stress exponent close to one, corresponding to its good creep resistance.

In addition to the relationship between the grain boundary phase and the high temperature mechanical properties of the duophase sialon, the development of elongated grains was also of interest for the following reasons: (1) Some of the elongated grains were highly faulted and rich in aluminum, not normal Si-rich Si-Al-O-N sialon grains. From the XRD results, the faulted elongated grains are a zeta-$Si_3Al_7O_3N_9$ aluminum silicon oxide nitride phase. (2) The elongated grains might be able to improve the toughness and creep resistance of the materials. (3) Too many elongated grains might degrade the flexure strength. Further experiments are underway to explore the new phase, ways to control the growth of elongated grains, and their correlation with the mechanical properties.

CONCLUSIONS

A duophase (α'/β') sialon for high temperature ceramic turbine engine application has been developed to have the following properties:

Density	3.25 g/cm^3
Hardness	20.5 MPa
Fracture Toughness	5.5 MPa-m$^{1/2}$
4-pt Flexural Strength	
25°C	670 MPa
1200°C	510 MPa
1300°C	490 MPa
1370°C	490 MPa
Flexural Stress Rupture	
1300°C, 240 MPa	No failure after 190 hrs
Strain rate	0.0010%/hr
1300°C, 340 MPa	No failure after 190 hrs
Strain rate	0.0014%/hr

The grain boundary phases played an important role in controlling the high temperature mechanical properties of this duophase sialon. Optimum post-sintering thermal treatment improved the flexural strength from 350 MPa to 490 MPa at 1300°C and 1370°C. This was due to the formation of isolated and crystallized yttrium-rich refractory grain boundary phases.

The creep behavior of the duophase sialon was affected by the crystallized grain boundary phase, α'/β' content and grain morphology. The formation of a YAG grain boundary phase and elongated grains yielded better creep resistance.

ACKNOWLEDGEMENTS

This work was carried out under contract to Allison Gas Turbine Division of General Motors Corp. sponsored by the U.S. Department of Energy. The authors acknowledge Mr. Gilbert Rancoule of Vesuvius Crucible and Dr. Ian Wilson of Vesuvius Zyalon for their helpful technical discussion. Research sponsored in part by the U.S. Department of Energy, Assistant Secretary for Conservation and Renewable Energy, Office of Transportation Technologies, as part of the High Temperature Materials Laboratory User Program, under contract DE-AC05-840R21400 with Martin Marietta Energy Systems, Inc.

REFERENCE

1. Proceedings of the Annual Automotive Technology Development Contractors' Meeting, Society of Automotive Engineers, Inc. Dearborn, Michigan, October 22-25, 1990

2. Helms H.E., Haley P.J., Groseclose L.E., Hilpisch S.J. and Bell A.H.III., Advanced Turbine Technology Applications Project (ATTAP). in Proceeding of the Annual Automotive Technology Development Contractors' Meeting, Society of Automotive Engineers, Inc. Dearborn, Michigan, October 22-25, 1990, pp.89-103.

3. Prochazka S. and Rocco W.A., High Pressure Hot Pressing of Silicon Nitride Powders. in Nitrogen Ceramics, edited by Riley F.L., Noordhoff. Netherlands, 1981

4. Clarke D.R., Lange F.F. and Shnitgrund G.D., Strengthening of Sintered Silicon Nitride by Post-fabrication Heat Treatment. J. Am. Ceram. Soc. 1982, 4, C51-C52

5. Jack K.H., Crystal Chemistry of SiAlONs and Related Nitrogen Ceramics. in Nitrogen Ceramics. Edited by F.L. Riley, Noordhoff, Netherlands, 1977

6. Aucote J. and Foster S.R., Performance of sialon Cutting Tools When Machining Nickel-Base Aerospace Alloys. Met. Sci. Technol., 1986, 2, 700-708.

7. Novich B.E., Lee R.-R., Franks G., and Ouellette D., Quickset™ Injection Molding of High Temperature Gas Turbine Engine Components. in Proceeding of the Annual Automotive Technology Development Contractors' Meeting, Society of Automotive Engineers, Inc. Dearborn, Michigan, October 23-26, 1989, pp.311-318.

8. Novich B.E., Lee R.-R., Franks G., Ouellette D., and Groseclose L.E., Ceramic Engine Components Fabricated by Using the Quickset Injection Molding Process. in 4th International Symposium on Ceramic Materials & Components for Engines., Goteborg, Sweden, June 10-12, 1991, published in this issue.

9. Chantikul P., Anstis G.R., Lawn B.R. and Marshall D.B., A Critical Evaluation of Indention techniques for Measuring Fracture Toughness: II Strength Method. J. Am. Ceram. Soc., vol.64, 9, 1981, PP.539-543.

10. Hollenburg, G.W., Terwilliger G.R., and Gordon R.S., Calculation of Stresses and Strain in Four-point Bending Creep Tests. J. Am. Ceram. Soc., Vol.54, 4, 1971, pp 196-99

11. Riedel H., Fracture at High Temperature, Springer-Verlag, Berlin, Heidelburgh, 1987

12. Lee R.-R., unpublished work.

13. Land P.L., Wimmer J.M. Burns, R.W., and Chourhury N.S., Compounds and Properties of the Systems Si-Al-O-N, J. Am. Ceram. Soc., Vol.61, 1-2, 1987, pp 56

DISCLAIMER

END

DATE FILMED

10/25/91